PCCP

RSC Publishing

PAPER

View Article Online
View Journal | View Issue

Detection of a charge-separated catalyst precursor state in a linked photosensitizer-catalyst assembly†

Cite this: *Phys. Chem. Chem. Phys.*, 2013, **15**, 21070

Anusree Mukherjee,[a] Oleksandr Kokhan,[a] Jier Huang,[a] Jens Niklas,[a] Lin X. Chen,*[ab] David M. Tiede[a] and Karen L. Mulfort*[a]

Received 18th October 2013,
Accepted 6th November 2013

DOI: 10.1039/c3cp54420f

www.rsc.org/pccp

We have designed two new supramolecular assemblies based on Co(II)-templated coordination of $Ru(bpy)_3^{2+}$ (bpy = 2,2′-bipyridyl) analogues as photosensitizers and electron donors to a cobaloxime macrocycle, which are of interest as proton reduction catalysts. The self-assembled photocatalyst precursors were structurally characterized by Co K-edge X-ray absorption spectroscopy and solution-phase X-ray scattering. Visible light excitation of one of the assemblies has yielded instantaneous electron transfer and charge separation to form a transient Co(I) state which persists for 26 ps. The development of a linked photosensitizer–cobaloxime architecture supporting efficient Co(I) charge transfer is significant since it is mechanistically critical as the first photo-induced electron transfer step for hydrogen production, and has not been detected in previous photosensitizer–cobaloxime linked dyad assemblies. X-band EPR spectroscopy has revealed that the Co(II) centres of both assemblies are high spin, in contrast to most previously described cobaloximes, and likely plays an important role in facilitating photoinduced charge separation. Based on the results obtained from ultrafast and nanosecond transient absorption optical spectroscopies, we propose that charge recombination occurs through multiple ligand states present within the photosensitizer modules. The studies presented here will enhance our understanding of supramolecular photocatalyst assembly and direct new designs for artificial photosynthesis.

Introduction

The development of materials that can sustainably and efficiently convert solar energy to chemical energy stored within the bonds of small molecules such as hydrogen is an enormous scientific and technical challenge.[1–3] Bio-inspired approaches toward artificial photosynthesis have yielded numerous molecular structural analogues to naturally occurring active sites, many of which notably contain only earth-abundant elements.[4–8] Additionally, supramolecular architectures present unique opportunities to tune chromophore-catalyst coupling and introduce mechanisms for self-repair. However, outside the framework of a protein structure, discrete homogeneous photocatalysts often suffer from poor stability and longevity or are unable to sustain the long-lived photo-induced charge separation necessary to initiate substrate binding. Nevertheless, homogeneous molecular and supramolecular architectures are well-positioned to make a huge impact in the pursuit of new materials for artificial photosynthesis since their ground and excited state structures are readily probed by both traditional and emerging physical characterization techniques. New molecular and supramolecular design and discovery will accelerate knowledge of the relevant formation and degradation pathways, desirable and unproductive electron transfer pathways, and facilitate comprehensive mapping of structure-function behaviour.

Among molecular compounds for proton reduction catalysis, cobaloximes have received special attention,[9–14] largely because of their relatively low overpotential.[15] Additionally, the cobaloxime macrocycle architecture presents many possible sites to couple photosensitizers to initiate H_2 catalysis by visible light. In particular, supramolecular coordination of pyridyl-functionalized photosensitizers directly to the axial position of the cobalt macrocycle Co(II) site has been a common tactic in building cobaloxime-based photocatalysts. The original design[16] and several follow-up contributions[17,18] was intended to overcome diffusion limited photoinduced electron transfer (PET) to the

[a] *Division of Chemical Sciences and Engineering, Argonne National Laboratory, 9700 South Cass Avenue, Argonne, IL 60439, USA. E-mail: mulfort@anl.gov; Fax: +1 630 252 9289; Tel: +1 630 252 3545*

[b] *Department of Chemistry, Northwestern University, 2145 Sheridan Road, Evanston, Illinois, 60208, USA. E-mail: lchen@anl.gov*

† Electronic supplementary information (ESI) available: Full synthetic details and standard characterization of **RuL1**, **RuL2**, assemblies **1** and **2**. Complete experimental results of EPR spectroscopy, X-ray absorption spectroscopy, X-ray scattering, ultrafast transient optical spectroscopy, nanosecond transient optical spectroscopy. See DOI: 10.1039/c3cp54420f

catalytic centre, but in general axial photosensitizer coordination to the cobaloxime macrocycle does not significantly improve total H_2 TONs when compared to analogous multi-molecular systems. Detailed structural studies using ^{1}H NMR[19] and solution-phase X-ray scattering[20] have demonstrated and quantified the lability of the photocatalyst assembly motif. Furthermore, our comprehensive transient optical spectroscopy[20] and EPR studies[21] suggest that the axial coordination of these supramolecular designs may actually inhibit the catalytically-active Co(I) charge-separated (CS) state by promoting fast back electron transfer to quickly regenerate the photosensitizer ground state. Accumulation of the Co(I) state has been observed at long time scales in multi-component systems,[22,23] and more recently, in a donor–donor–cobaloxime triad assembly.[24] However, the vast majority of linked photosensitizer–cobaloxime assemblies have not demonstrated formation of this first crucial catalytic intermediate.

In this report, we describe a new supramolecular approach to link cobaloxime H_2 catalyst modules with visible-light absorbing photosensitizers using metal-templated macrocycle formation (Scheme 1). The photocatalyst precursors described here represent a significant departure from the axial coordination of current cobaloxime-based assemblies and instead target equatorial photosensitizer coordination through elaboration of the glyoxime macrocycle. Remarkably, this ligand manifold enables apparently *instantaneous* formation of the Co(I) charge-separated state, the key intermediate relevant to H_2 catalysis by cobaloximes. Also, two different photosensitizer-catalyst bridges have allowed us to modulate the physical and electronic coupling which governs the fundamental steps relevant to artificial photosynthesis.

Results

Synthesis

Two new cobaloxime-based supramolecular assemblies were successfully synthesized *via* glyoxime functionalization of Ru(II)-tris(bipyridyl) light-harvesting compounds (Scheme 1). Full synthesis details are available in the ESI,† but briefly, glyoxime-functionalized phenanthroline ligands (**L1** and **L2**) were prepared by acid-catalysed chlorination of either glyoxime or 3-methyl glyoxime at low temperature followed by substitution with the bis- or mono-substituted amine. The Ru(II)-tris(bipyridyl) compounds (**RuL1**, **RuL2**) were then obtained by typical ligand exchange conditions from $Ru(bpy)_2Cl_2{\cdot}2H_2O$ and structurally characterized by ^{1}H NMR, ESI-MS, absorbance and emission spectroscopies, and cyclic voltammetry (see ESI†). Self-assembly to form the equatorially-linked cobaloxime-based photocatalyst precursors **1** and **2** was achieved simply by adding a stoichiometric amount of $CoCl_2$ to solutions of **RuL1** and **RuL2** in acetone followed by solvent removal under reduced pressure. X-band EPR spectroscopy of assembly **1** in 3 : 1 CH_2Cl_2 : CH_3CN at 7.5 K showed a broad signal with two effective g values around 4.7 and a third at 2.3, characteristic of the presence of high spin Co(II) in an octahedral environment with two anionic axial ligands.

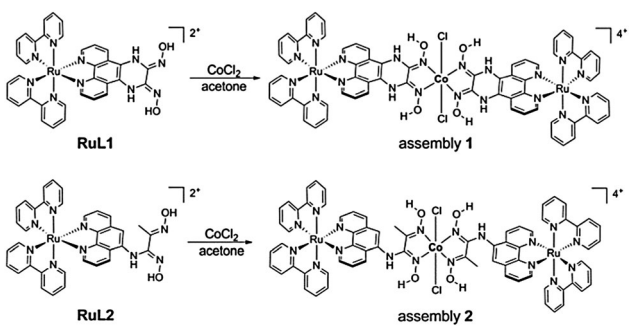

Scheme 1 Chemical structure of photosensitizer modules **RuL1** and **RuL2** and Co(II)-templated assemblies **1** and **2**.

X-ray characterization of assemblies 1 and 2

Supramolecular assemblies are often difficult to characterize by conventional methods; mass spectrometry can disrupt structures held together by relatively weak interactions and NMR is useful for detecting local coordination events but it can be quite difficult to assess global structural features.[25] Therefore, we turned to synchrotron X-ray based techniques[26] to characterize both the local and global structure of assemblies **1** and **2**. First, the local cobalt coordination geometry and macrocycle integrity was characterized by X-ray absorption spectroscopy at the cobalt K-edge. X-ray absorption near edge structure (XANES) spectra of **1** confirmed that the oxidation state of the cobalt centre remained in the +2 state following assembly, showing the transition edge energy observed at 7721.5 eV, typical for a Co(II) complex in an octahedral environment.[27] The pre-edge features of assembly **1** due to the weak quadrupole 1s → 3d transition further confirmed the expected octahedral Co(II) coordination geometry. Similar analysis of **2** yielded an absorption edge between that of Co(II) and Co(III) standards and suggests the coexistence of both oxidation states for this assembly. X-ray absorption fine structure (XAFS) data analysis of **1** revealed the cobalt–ligand distances of the first coordination shell. Fitting the XAFS data resulted in four Co–N bonds (2.05 Å) and two Co–Cl bonds (2.29 Å) which agree well with an energy-minimized model and crystal structure data of model compounds.[28]

Solution-phase X-ray scattering was used to characterize the global structure of assemblies **1** and **2** in relatively dilute solutions in CH_3CN. The scattering pattern of the solute alone was obtained following subtraction of the neat solvent scattering response from the sample pattern. Guinier analysis of small-angle X-ray scattering is a fairly common technique to obtain the radius of gyration (R_g) of uniform, homogeneous particles in solution.[29] R_g is related to the scattering intensity at low q values through the relationships

$$I(q) = I(0)\exp\left(\frac{q^2 R_g^2}{3}\right) \quad (1)$$

$$I(0) = [C]V_m^2(\rho_m - \rho_0)^2 \quad (2)$$

where $I(0)$ is the scattering intensity at $q = 0$, C is the concentration of the assembly, V_m is the total excluded solvent volume of the scatterer, ρ_m and ρ_0 are the average electron density of the scatterer and solvent, respectively. We measured the small-angle

Table 1 Summary of Guinier analysis of photosensitizer modules and assemblies at 5 mM in CH_3CN

	Model R_g (Å)	Experiment R_g (Å)
RuL1	6.58	6.57 ± 0.08
Assembly **1**	10.70	10.65 ± 0.18
RuL2	6.12	6.10 ± 0.11
Assembly **2**	10.33	10.09 ± 0.16

X-ray scattering patterns from **RuL1**, assembly **1**, **RuL2**, and assembly **2** at 5 mM in CH_3CN and found excellent agreement between the values obtained experimentally and those from simulated coordinate-based scattering patterns from energy-minimized models (Table 1).[30] As expected, Guinier analysis of the scattering from assemblies **1** and **2** results in significantly larger R_g values than the light-harvesting modules alone and confirms assembly formation in solution.

Transient optical spectroscopy

Following confirmation of supramolecular assembly of **1** and **2**, femtosecond and nanosecond transient optical spectroscopy were used to probe the kinetics of photoexcitation and charge separation. Based on analysis of the optical and redox properties of **RuL1** and **RuL2**, the driving force for PET in assemblies **1** and **2** are nearly identical. However, the transient spectra and kinetics of assemblies **1** and **2** display striking differences, particularly in the first 100 ps following photoexcitation. Excitation of the metal-to-ligand charge transfer (MLCT) transition of **RuL1** at 420 nm resulted in formation of the ground state bleach (GSB) band <500 nm and a broad band centred at 600 nm associated with excited state absorption (ESA), typical of $Ru(bpy)_3^{2+}$-type compounds (Fig. 1A).[31] Following very fast sub-picosecond quench of the ESA due to intersystem crossing, the kinetics of ESA decay at 570 nm remained flat, suggesting a long lived excited state, well beyond the timescale of the ultrafast experiment. Complementary nanosecond spectroscopy of **RuL1** yielded ESA decay at 570 nm with a lifetime of 558 ns. In stark contrast, the transient spectra of assembly **1** displayed instantaneous formation of an outstanding spectral feature between 520–600 nm (Fig. 1B). This feature correlates with the spectrum of the Co(I) reduced state of the cobaloxime macrocycle, confirmed by spectroelectrochemistry of a cobaloxime model compound (Fig. S14, ESI†).[32,33] Global fitting of the ultrafast and nanosecond kinetics of **1** in CH_3CN yielded a multi-exponential decay at 570 nm with time constants τ_1 = 26 ps, τ_2 = 3 ns, and τ_3 = 246 ns (see ESI† for complete fitting details).

To confirm the nature of the ultrafast feature observed in assembly **1**, two control spectroscopy experiments were performed. In the first, electronically inert Zn(II) was used to form a metal-templated assembly with the appropriate stoichiometry (2 : 1 **RuL1** : $ZnCl_2$). The Zn(II) analogue of assembly **1** displayed a broad ESA band nearly identical to that of **RuL1** alone with similar kinetics (Fig. S18, ESI†). In the second control, a $Ru(bpy)_3^{2+}$ analogue without glyoxime functionality, $Ru(bpy)_2$(5-amine-1,10-phenanthroline)·$2PF_6$, was mixed with $CoCl_2$ in a 2 : 1 ratio to test the effect of cobalt macrocycle formation. In the ultrafast experiment, a broad ESA was observed, again similar to that of **RuL1** alone in CH_3CN.

No evidence of the Co(I) CS state was observed following visible excitation of assembly **2**. In both the ultrafast and nanosecond time scales, the transient spectra of assembly **2** resemble the spectral features of **RuL2** alone and exhibit similar kinetic parameters (Fig. S21, ESI†).

Discussion

Synthesis of new, appropriately functionalized light-harvesting modules has enabled us to access supramolecular structures which have potential as photocatalysts for proton reduction catalysis. In addition to characterization of the modules by standard methods, we have used complementary synchrotron X-ray techniques to probe both the local Co(II)-macrocycle structure by XAS and the global structure of the assembly structure by Guinier analysis of the SAXS patterns. The results

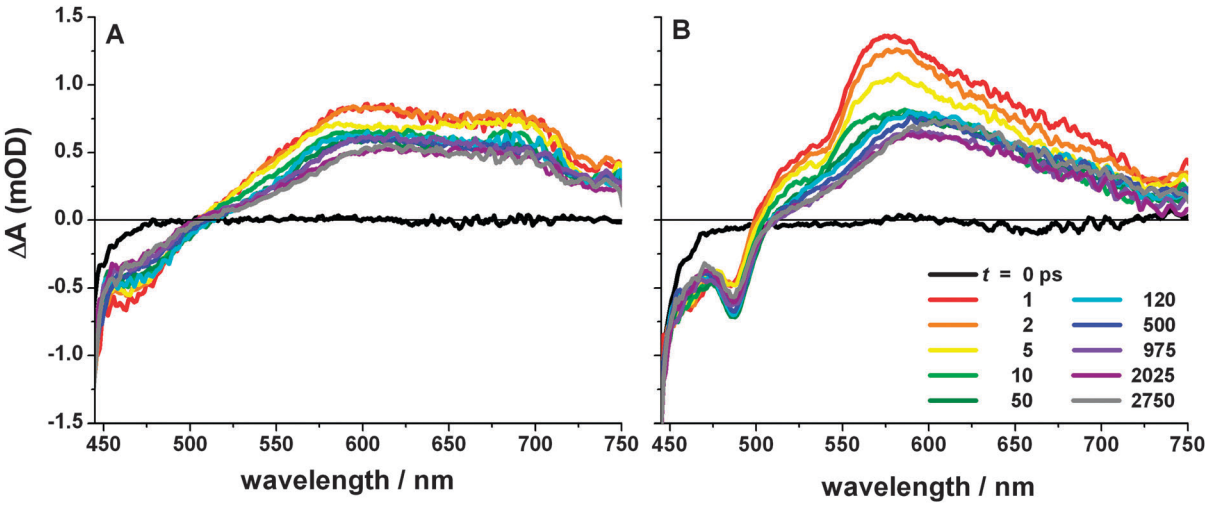

Fig. 1 Comparison of ultrafast transient optical spectra of (A) **RuL1** and (B) assembly **1** at identical optical density in CH_3CN. Pump wavelength 420 nm.

firmly establish the formation of the expected cobaloxime macrocycle and overall supramolecular structure by metal-mediated self-assembly.

A combination of femtosecond and nanosecond transient optical spectroscopies were used to investigate the behaviour of the light-harvesting modules and equatorially-coordinated cobaloxime-based assemblies. Following visible excitation of **RuL1** in CH_3CN, mono-exponential decay of the ESA and recovery to ground state with τ = 558 ns (τ_{GS1}) was observed. This is consistent with $Ru(bpy)_3^{2+}$-type compounds, and explained by MLCT to a distinct low-lying π^* acceptor level within the **L1** ligand. The electron acceptor in the form of the cobaloxime macrocycle in assembly **1** results in additional complexities to the transient components. The energy level diagram based on the relative donor–acceptor energy levels which explains our kinetic model for assembly **1** is shown in Fig. 2. The simplest solution that describes the multi-exponential decay kinetics and correlates with the relevant donor–acceptor energy levels is a system of five linear differential equations, which is in excellent agreement with the fit to experimental data (Fig. S17, ESI†). From ***RuL1**, the excited electron has two possible decay pathways: the first through $MLCT_1$, which is localized on the **L1** phenanthroline ligand as observed in native photosensitizer **RuL1**, and the other is localized on the cobaloxime which yields the catalytically-relevant Co(I) CS state. In assembly **1** the $MLCT_1$ state recombines to ground state with τ_3 = 246 ns, a slight acceleration from **RuL1** alone, which may be the result of extended conjugation in **1** or slight changes in the electronic structure of **L1** following cation coordination. Formation of the Co(I) CS state occurs instantaneously within the resolution of the ultrafast spectroscopy experiment but decays rather quickly, with τ_1 = 26 ps. This fast decay of the Co(I) CS state and the relative energy levels of $MLCT_1$ and Co(II/I) lead us to propose the presence of another accessible ligand-centred MLCT state in assembly **1**. The presence of multiple MLCT states in a Ru(II)-polypyridyl ligand has been observed before in dppz (dipyrido[3,2-*a*:2′,3′-*c*]-phenazine), which is structurally similar to **L1**.[34,35] The $MLCT_1$ level of dppz is observed in the absorbance spectrum and centred on the phenanthroline portion, and the $MLCT_0$ level is observed in the emission spectrum and centred on the pyrazine portion.[36] In the fully conjugated dppz, initial photoexcitation to $MLCT_1$ is followed by fast, solvent dependent, intraligand electron transfer to $MLCT_0$ which then decays to ground state on the typical time scale for $Ru(bpy)_3^{2+}$ compounds. The multi-exponential decay observed following visible excitation of assembly **1** closely resembles this process. Following instantaneous formation of the Co(I) CS state, charge recombination with τ_1 = 26 ps occurs to the saturated pyrazine centred $MLCT_0$ state which then decays with τ_2 = 3 ns.

The two control spectroscopy experiments are crucial to unambiguous determination of the instantaneous CS state observed in **1**. The marked contrast between photoinduced spectra in the 520–600 nm region of **1** and 2 : 1 **RuL1** : $ZnCl_2$ demonstrates that the transient spectra of **1** arise from cobaloxime macrocycle

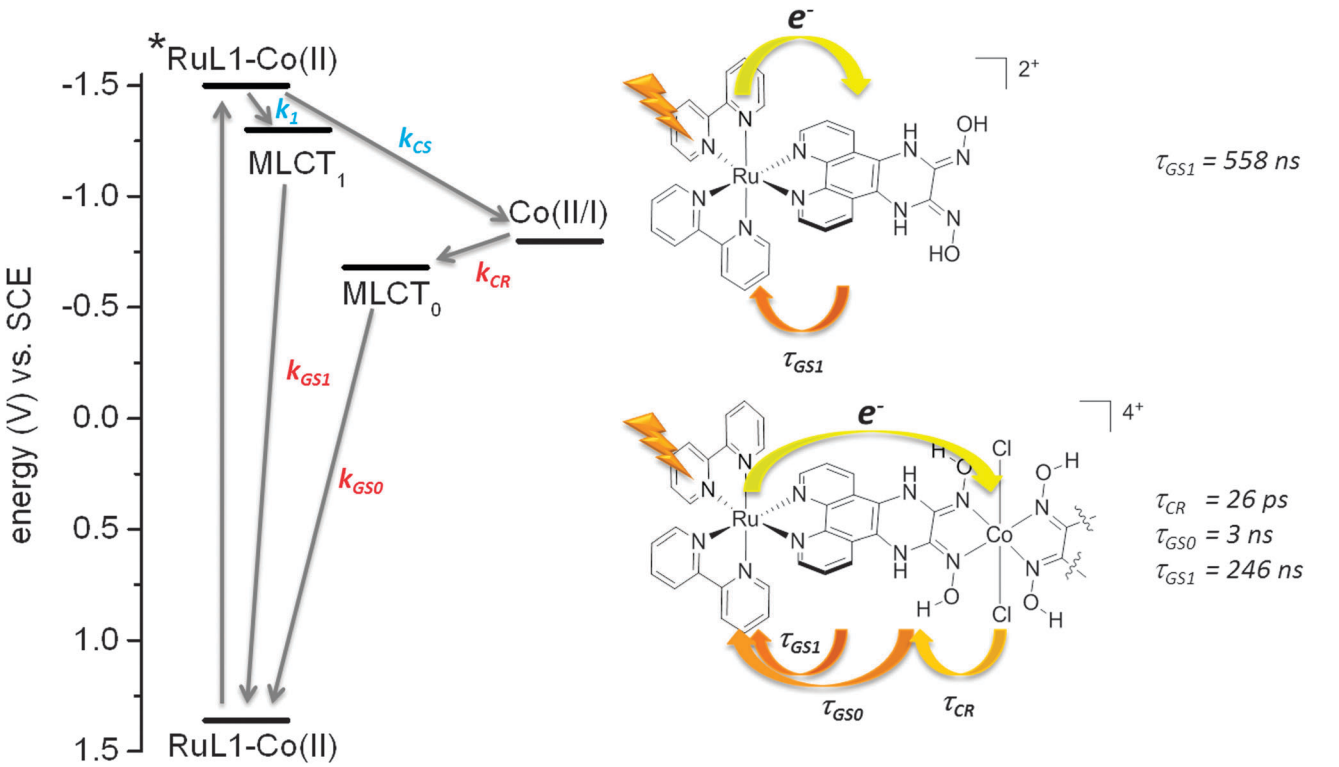

Fig. 2 Proposed energy level diagram following visible light excitation in CH_3CN of **RuL1** and assembly **1** from combined ultrafast and nanosecond spectroscopies. Rate constants in blue (k_1, k_{CS}) are not observed on ultrafast timescale, $MLCT_1$ spectra in **RuL1** and Co(I) CS spectra in assembly **1** are observed instantaneously following excitation. See ESI† for complete fitting details.

formation, not disruption of the **RuL1** MLCT levels following cation coordination. Additionally, visible excitation of 2 : 1 $Ru(bpy)_2$(5-amino-1,10-phenanthroline)·$2PF_6$: $CoCl_2$ led to similar ultrafast ESA decay kinetics as $Ru(bpy)_2$(5-amino-1,10-phenanthroline)·$2PF_6$ and **RuL1** alone. From this we conclude that the transient spectra of **1** do not arise from bimolecular energy transfer, which might be a consideration given the spectral overlap of Ru(II)-based emission and $CoCl_2$-based absorption. These two observations, as well as the assignment of Co(I) by spectroelectrochemistry, confirm the instantaneous PET to the self-assembled cobaloxime macrocycle.

Unlike the encouraging transient spectra of assembly **1**, no distinct evidence of the Co(I) state was observed following visible excitation of assembly **2**. In both the ultrafast and nanosecond time scales, the spectral features of assembly **2** resemble the spectral features of **RuL2** alone and exhibit similar kinetic parameters (Fig. S21, ESI†). The lack of observed CS to obtain the mechanistically-relevant Co(I) state in assembly **2** could be a result of either (1) the flexible **L2** ligand and break in conjugation between electron donor and acceptor prohibits forward electron transfer, or (2) the cobalt oxidation state in assembly **2** is intermediate between +2 and +3, as suggested by the ground state XANES spectroscopy (Fig. S9, ESI†). Additionally, the structure-function analysis of assembly **2** is likely complicated by a mixture of *cis–trans* isomerization of the **RuL2** module around the macrocycle.

There are several aspects that we considered in the design of assemblies **1** and **2** that we now know are critical to the PET characteristics and suspect may be relevant to their performance as potential H_2 photocatalysts. By appending the photosensitizer to the equatorial positions of the macrocycle, we drastically altered the cobalt coordination sphere from typical cobaloxime-based supramolecular assemblies and allowed two anionic ligands in the axial positions which strongly influence the cobalt spin state. As noted above, X-band EPR spectroscopy of assembly **1** gave a broad signal with two effective g values around 4.7 and a third at 2.3, supporting the presence of high spin Co(II) in an octahedral environment with two anionic axial ligands. This has been observed in similar cobalt complexes[37–40] but signifies a profound departure from the axially-coordinated cobaloxime macrocycles reported thus far[21,41,42] and likely explains the instantaneous photoinduced CS in **1** to yield the Co(I) centre. Both axial and equatorial coordination of photosensitizers to cobaloximes contain cobalt in the +2 oxidation state with $3d^7$ electronic configuration. In order for a low-spin Co(II) species to accept an electron, it must reside in an anti-bonding e_g orbital ($t_{2g}^6e^*_g{}^1 \rightarrow t_{2g}^6e^*_g{}^2$). However, in a high-spin complex, the reducing electron can populate the non-bonding t_{2g} level ($t_{2g}^5e^*_g{}^2 \rightarrow t_{2g}^6e^*_g{}^2$), which is energetically more favourable than electron transfer to an anti-bonding orbital. Therefore, the high spin state of the equatorially-coordinated assemblies here promotes instantaneous PET and CS to the Co(II) macrocycle which is not observed with axially-coordinated photosensitizers. In support of this hypothesis, similar electronic behaviour was attributed to a model complex of the oxygen evolution reaction, where the presence of an electron in an anti-bonding orbital explains the high catalytic activity of cobalt or manganese oxides.[43]

The instantaneous formation of the Co(I) CS state upon excitation of the **RuL1** MLCT transition is a remarkable feature of assembly **1**. Analogous instantaneous formation of CS[44–48] and extensively delocalized excited-states involving multiple redox chromophores has been observed by optical excitation of transition moments that are localized on single chromophores in photosynthetic reaction centre proteins.[45] In this way, we note that we have succeeded in creating an artificial assembly that duplicates the charge transfer character of the initial excited state produced in the primary electron transfer reactions in photosynthesis.

Conclusions

Here we have described the synthesis, structural characterization, and transient optical spectroscopy of two new supramolecular photosensitizer-catalyst assemblies which feature light-harvesting components equatorially coordinated to a cobaloxime macrocycle. By transforming the supramolecular scaffold from axial coordination directly to Co(II) to equatorial coordination through the cobaloxime macrocycle, we have observed visible light induced formation of the Co(I) charge-separated state, the key species responsible for catalytic proton reduction. The instantaneous formation of the charge-separated state in assembly **1** is reminiscent of the first steps following light absorption in photosynthesis, and draws a direct connection between natural photosynthesis and artificial architectures. Currently, we cannot definitively identify the source of the short-lived nature of the charge-separated state, or why we observe multiple ligand states in assembly **1**. However, the proposed kinetic model explains our experimental results well, and the presence of multiple ligand states likely explains the negligible H_2 photocatalytic efficiency of assembly **1**. Therefore, we note the fundamental importance of this observation but acknowledge that this intermediate has a relatively short lifetime, and an immediate research goal is to significantly enhance its stability.

Experimental section

All commercial reagents and solvents were purchased from Sigma-Aldrich and used without further purification unless otherwise noted. The synthesis of dichloroglyoxime, 5-nitro-6-amino-1,10-phenanthroline, $[Ru(bpy)_2$(5-nitro-6-amino-1,10-phenanthroline)·$2PF_6]$[49] and $[Ru(bpy)_2$(5,6-diamino-1,10-phenanthroline)·$2PF_6]$[50] was reported elsewhere. Complete synthesis details are in the ESI.† ^{1}H NMR was performed on a Bruker DMX 500 and referenced to TMS or residual solvent peak. ESI-MS was collected on a ThermoFisher LCQ Fleet, from dilute CH_3CN or methanol solutions in positive ionization mode. UV-Vis absorption measurements were performed on a Shimadzu UV-1601 spectrophotometer. Steady state emission spectra were measured on a Quantamaster spectrophotometer from Photon Technology International; each sample was dissolved in spectrophotometric grade CH_3CN with optical density ≤ 0.3 at the excitation wavelength and thoroughly de-aerated with N_2.

Cyclic voltammetry

Cyclic voltammetry was conducted using a standard three-electrode cell on a BioAnalytical Systems (BAS) 100B potentiostat and cell stand with a 3 mm-diameter glassy carbon working electrode, a Pt wire auxiliary electrode, and a pseudo Ag/AgCl reference electrode.[51] Each solution in anhydrous CH_3CN was purged with N_2 prior to measurement and subsequently maintained under a blanket of N_2. Tetrabutylammonium hexafluorophosphate (0.1 M) was used as the supporting electrolyte. Ferrocene (purified by sublimation) was added as an internal standard and redox potentials were referenced to the ferrocene/ferrocenium couple (0.40 V *vs.* SCE (CH_3CN)).[52] All scans were performed at 100 mV s^{-1}.

Spectroelectrochemistry

Spectroelectrochemistry was performed on the model compound $Co(dmgH)(dmgH_2)Cl_2$ in 1 : 1 H_2O : CH_3CN. A 1 mM solution of $Co(dmgH)(dmgH_2)Cl_2$ in 0.1 M KCl supporting electrolyte was purged with N_2 and placed in a quartz cuvette spectroelectrochemical cell (BAS) under N_2 atmosphere. The working (Pt mesh), auxiliary (PTFE-coated Pt wire), and reference (Ag/AgCl 3 M NaCl) electrodes were positioned in the cuvette using a Teflon cap, the cuvette was sealed with parafilm and then placed in the spectrophotometer. The potential was held at −600 and −1000 mV (*vs.* Ag/AgCl) to monitor the spectral changes at the Co(III/II) and Co(II/I) transitions, respectively.

Transient absorption spectroscopy

Ultrafast transient absorption spectroscopy was measured at the Center for Nanoscale Materials at Argonne National Laboratory using an amplified Ti:sapphire laser system (Spectra Physics, Spitfire-Pro) and an automated data acquisition system (Ultrafast Systems, Helios for 0–3 ns and EOS for 0–50 ns). The amplifier was seeded with the 120 fs output from the oscillator (Spectra Physics, Tsunami) and was operated at 1.66 kHz (1.0 kHz for EOS). The output from the amplifier was split 90/10 with the majority used to pump an optical parametric amplifier (Topas) which provided the pump beam. For Helios experiments, the 10% output was used to generate a continuum (450–750 nm) probe in sapphire; whereas for EOS, a supercontinuum light source (Ultrafast Systems) was used for the probe. The TA system collects two dimensional data (kinetics/spectra (ΔOD)) for probe wavelengths of 450–750 nm. For transient absorption spectroscopy each sample was dissolved in CH_3CN with optical density <0.4 at the pump wavelength. Samples were thoroughly deaerated with N_2 in a 2 mm cuvette and magnetically stirred during data collection. All measurements were made using 420 nm laser excitation, typical pulse energy was 275 nJ per pulse.

Single wavelength kinetic traces in the range of 30 ns–3 μs were recorded for the same deaerated samples in CH_3CN pumped at 460 nm using the output of an optical parametric oscillator pumped with third harmonic of a NdYAG laser (Surelite-II, Continuum). The width of the pump pulses was approximately 5 ns. Single wavelength kinetic traces were obtained using a white pulsed Xe lamp ($\tau \sim 50$ μs) as a probe source, Triax-180 monochromator (Horiba Jobin Yvon), and a PMT with its output digitized with a Picoscope 4227 (12-bit resolution, 250 MS s^{-1} sampling rate). The instrument response time was about 10 ns.

EPR spectroscopy

CW X-band (9.3 GHz) EPR experiments were carried out with a Bruker ELEXSYS E580 EPR spectrometer (Bruker Biospin, Rheinstetten, Germany), equipped with a TE_{102} rectangular EPR resonator (Bruker ER 4102st) and a helium gas-flow cryostat (Air Product, Allentown, PA). The temperature was maintained at 7.5 K by a Lakeshore cryogenic temperature controller (Westerville, OH). Several EPR spectra were recorded with different microwave powers to ensure non-saturating conditions. Data processing was done using Xepr (Bruker BioSpin, Rheinstetten); background signals as obtained by measuring a sample containing only solvent were subtracted.

X-ray absorption data collection and analysis

The cobalt K-edge X-ray absorption spectra of assembly **1** and **2** in CH_3CN (5 mM) were collected at beamline 12-BM of the Advanced Photon Source, Argonne National Laboratory. At beamline 12-BM, the radiation was monochromatized by Si(111) double crystals. The spectra were collected in fluorescence detection mode, using a Canberra 13-element solid-state germanium detector array, with the fluorescence photon energy window set for the cobalt Kα emission. A cobalt foil was placed in between two ionization chambers after the sample and used as references for the *in situ* energy calibration. XAFS data analysis was performed with the Athena and Artemis packages based on FEFF programs.

Solution phase X-ray scattering data collection and analysis

X-ray scattering data were acquired on **RuL1**, **RuL2**, assembly **1**, and assembly **2** at 5 mM concentration in CH_3CN at beamline 12-ID-B of the Advanced Photon Source of Argonne National Lab. Pilatus 2 M detector was used for collecting small-angle X-ray scattering data and provided q range coverage from 0.075 $Å^{-1}$ to 0.80 $Å^{-1}$. Wide-angle X-ray scattering data were acquired with Pilatus 300k detector and had a q range of 0.85–2.3 $Å^{-1}$. Typically, 20 sequential images were collected with 2 s exposure time per image with each detector. q range calibration was performed with a silver behenate sample. The blank solvent scattering data were subtracted from sample data and the solvent peak (CH_3CN appears near $q = 1.65$ $Å^{-1}$) was used as a control in subtractions to obtain the scattering pattern from the solute alone.

Acknowledgements

We acknowledge funding from the Division of Chemical Sciences, Biosciences, Office of Basic Energy Sciences of the U.S. Department of Energy through Grant DE-AC02-06CH11357 for support of this work. Use of the Center for Nanoscale Materials was supported by the U.S. Department of Energy, Office of Science, Office of Basic Energy Sciences, under Contract No. DE-AC02-06CH11357. We thank Dr David J. Gosztola for his expert assistance at the transient absorption facility at CNM. Use of beamlines 12-BM (XAS) and 12-ID-B (X-ray scattering)

at the Advanced Photon Source, an Office of Science User Facility operated for the U.S. Department of Energy Office of Science by Argonne National Laboratory, was supported by the U.S. DOE under Contract No. DE-AC02-06CH11357.

Notes and references

1 N. S. Lewis and D. G. Nocera, *Proc. Natl. Acad. Sci. U. S. A.*, 2006, **103**, 15729.
2 H. B. Gray, *Nat. Chem.*, 2009, **1**, 7.
3 J. L. Dempsey, B. S. Brunschwig, J. R. Winkler and H. B. Gray, *Acc. Chem. Res.*, 2009, **42**, 1995.
4 F. Gloaguen and T. B. Rauchfuss, *Chem. Soc. Rev.*, 2009, **38**, 100.
5 D. M. Rakowski and D. L. DuBois, *Chem. Soc. Rev.*, 2009, **38**, 62.
6 V. Artero, M. Chavarot-Kerlidou and M. Fontecave, *Angew. Chem., Int. Ed.*, 2011, **50**, 7238.
7 P. Du and R. Eisenberg, *Energy Environ. Sci.*, 2012, **5**, 6012.
8 W. T. Eckenhoff and R. Eisenberg, *Dalton Trans.*, 2012, **41**, 13004.
9 P. Connolly and J. H. Espenson, *Inorg. Chem.*, 1986, **25**, 2684.
10 X. Hu, B. M. Cossairt, B. S. Brunschwig, N. S. Lewis and J. C. Peters, *Chem. Commun.*, 2005, 4723.
11 C. Baffert, V. Artero and M. Fontecave, *Inorg. Chem.*, 2007, **46**, 1817.
12 B. D. Stubbert, J. C. Peters and H. B. Gray, *J. Am. Chem. Soc.*, 2011, **133**, 18070.
13 M. Razavet, V. Artero and M. Fontecave, *Inorg. Chem.*, 2005, **44**, 4786.
14 P.-A. Jacques, V. Artero, J. Pecaut and M. Fontecave, *Proc. Natl. Acad. Sci. U. S. A.*, 2009, **106**, 20627.
15 X. Hu, B. S. Brunschwig and J. C. Peters, *J. Am. Chem. Soc.*, 2007, **129**, 8988.
16 A. Fihri, V. Artero, M. Razavet, C. Baffert, W. Leibl and M. Fontecave, *Angew. Chem., Int. Ed.*, 2008, **47**, 564.
17 A. Fihri, V. Artero, A. Pereira and M. Fontecave, *Dalton Trans.*, 2008, 5567.
18 C. Li, M. Wang, J. Pan, P. Zhang, R. Zhang and L. J. Sun, *J. Organomet. Chem.*, 2009, **694**, 2814.
19 T. M. McCormick, Z. Han, D. J. Weinberg, W. W. Brennessel, P. L. Holland and R. Eisenberg, *Inorg. Chem.*, 2011, **50**, 10660.
20 K. L. Mulfort and D. M. Tiede, *J. Phys. Chem. B*, 2010, **114**, 14572.
21 J. Niklas, K. L. Mardis, R. R. Rakhimov, K. L. Mulfort, D. M. Tiede and O. G. Poluektov, *J. Phys. Chem. B*, 2012, **116**, 2943.
22 J. L. Dempsey, J. R. Winkler and H. B. Gray, *J. Am. Chem. Soc.*, 2009, **132**, 1060.
23 P. Du, J. Schneider, G. Luo, W. W. Brennessel and R. Eisenberg, *Inorg. Chem.*, 2009, **48**, 4952.
24 B. S. Veldkamp, W.-S. Han, S. M. Dyar, S. W. Eaton, M. A. Ratner and M. R. Wasielewski, *Energy Environ. Sci.*, 2013, **6**, 1917.
25 A. Pastor and E. Martinez-Viviente, *Coord. Chem. Rev.*, 2008, **252**, 2314.
26 K. L. Mulfort, A. Mukherjee, O. Kokhan, P. Du and D. M. Tiede, *Chem. Soc. Rev.*, 2013, **42**, 2215.
27 M. D. Hall, C. K. Underwood, T. W. Failes, G. J. Foran and T. W. Hambley, *Aust. J. Chem.*, 2007, **60**, 180.
28 N. W. Alcock, M. P. Atkins, E. H. Curzon, B. T. Golding and P. J. J. Sellars, *J. Chem. Soc., Chem. Commun.*, 1980, 1238.
29 A. Guinier and G. Fournet, *Small-Angle Scattering of X-rays*, Wiley, New York, 1955.
30 D. Tiede, K. Mardis and X. Zuo, *Photosynth. Res.*, 2009, **102**, 267.
31 K. Kalyanasundaram, *Coord. Chem. Rev.*, 1982, **46**, 159.
32 O. Pantani, E. Anxolabéhère-Mallart, A. Aukauloo and P. Millet, *Electrochem. Commun.*, 2007, **9**, 54.
33 P. Zhang, P.-A. Jacques, M. Chavarot-Kerlidou, M. Wang, L. Sun, M. Fontecave and V. Artero, *Inorg. Chem.*, 2012, **51**, 2115.
34 S. Campagna, F. Puntoriero, F. Nastasi, G. Bergamini and V. Balzani, *Photochemistry and Photophysics of Coordination Compounds: Ruthenium Photochemistry and Photophysics of Coordination Compounds I*, ed. V. Balzani and S. Campagna, Springer, Berlin/Heidelberg, 2007, vol. 280, pp. 117–214.
35 C. Chiorboli, M. A. J. Rodgers and F. Scandola, *J. Am. Chem. Soc.*, 2003, **125**, 483.
36 R. López, A. M. Leiva, F. Zuloaga, B. Loeb, E. Norambuena, K. M. Omberg, J. R. Schoonover, D. Striplin, M. Devenney and T. J. Meyer, *Inorg. Chem.*, 1999, **38**, 2924.
37 P. C. Kang, G. R. Eaton and S. S. Eaton, *Inorg. Chem.*, 1994, **33**, 3660.
38 J. S. Park, T.-J. Park, K.-H. Kim, K. Oh, M.-S. Seo, H.-I. Lee, M.-J. Jun, W. Nam and K. M. Kim, *Bull. Korean Chem. Soc.*, 2006, **27**, 193.
39 D. Reinen, A. Ozarowski, B. Jakob, J. Pebler, H. Stratemeier, K. Wieghardt and I. Tolksdorf, *Inorg. Chem.*, 1987, **26**, 4010.
40 J. G. McAlpin, Y. Surendranath, M. Dinca, T. A. Stich, S. A. Stoian, W. H. Casey, D. G. Nocera and R. D. Britt, *J. Am. Chem. Soc.*, 2010, **132**, 6882.
41 G. N. Schrauzer and L. P. Lee, *J. Am. Chem. Soc.*, 1970, **92**, 1551.
42 A. Bakac, M. E. Brynildson and J. H. Espenson, *Inorg. Chem.*, 1986, **25**, 4108.
43 U. Maitra, B. S. Naidu, A. Govindaraj and C. N. R. Rao, *Proc. Natl. Acad. Sci. U. S. A.*, 2013, **110**, 11704.
44 A. R. Holzwarth, M. G. Muller, M. Reus, M. Nowaczyk, J. Sander and M. Rogner, *Proc. Natl. Acad. Sci. U. S. A.*, 2006, **103**, 6895.
45 L. Huang, N. Ponomarenko, G. P. Wiederrecht and D. M. Tiede, *Proc. Natl. Acad. Sci. U. S. A.*, 2012, **109**, 4851.
46 V. I. Novoderezhkin, E. Romero, J. P. Dekker and R. van Grondelle, *ChemPhysChem*, 2011, **12**, 681.
47 M. E. van Brederode and R. van Grondelle, *FEBS Lett.*, 1999, **455**, 1.
48 M. E. van Brederode, F. van Mourik, I. H. M. van Stokkum, M. R. Jones and R. van Grondelle, *Proc. Natl. Acad. Sci. U. S. A.*, 1999, **96**, 2054.
49 J. Bolger, A. Gourdon, E. Ishow and J.-P. Launay, *Inorg. Chem.*, 1996, **35**, 2937.
50 E. Ishow, A. Gourdon, J.-P. Launay, C. Chiorboli and F. Scandola, *Inorg. Chem.*, 1999, **38**, 1504.
51 P. H. Dinolfo, M. E. Williams, C. L. Stern and J. T. Hupp, *J. Am. Chem. Soc.*, 2004, **126**, 12989.
52 N. G. Connelly and W. E. Geiger, *Chem. Rev.*, 1996, **96**, 877.

